Critical Current Scaling and Anisotropy in Oxypnictide Superconductors

M. Kidszun,[1,2,*] S. Haindl,[1] T. Thersleff,[1] J. Hänisch,[1] A. Kauffmann,[1] K. Iida,[1] J. Freudenberger,[1] L. Schultz,[1,2] and B. Holzapfel[1,2]

[1]*IFW Dresden, Institute for Metallic Materials, P.O. Box 270116, 01171 Dresden, Germany*
[2]*TU Dresden, Institut für Festkörperphysik, 01069 Dresden, Germany*

(Received 8 December 2010; published 29 March 2011)

Having succeeded in the fabrication of epitaxial superconducting $LaFeAsO_{1-x}F_x$ thin films we performed an extensive study of electrical transport properties. In the face of multiband superconductivity we can demonstrate that an anisotropic Ginzburg-Landau scaling of the angular dependent critical current densities can be adopted, although being originally developed for single band superconductors. In contrast with single band superconductors the mass anisotropy of $LaFeAsO_{1-x}F_x$ is temperature dependent. A very steep increase of the upper critical field and the irreversibility field can be observed at temperatures below 6 K, indicating that the band with the smaller gap is in the dirty limit. This temperature dependence can be theoretically described by two dominating bands responsible for superconductivity. A pinning force scaling provides insight into the prevalent pinning mechanism and can be specified in terms of the Kramer model.

DOI: 10.1103/PhysRevLett.106.137001 PACS numbers: 74.70.Xa, 74.25.F−, 74.25.Sv, 74.25.Wx

Superconductivity in $LaFeAsO_{1-x}F_x$, hereafter La-1111, was discovered in 2008 by Kamihara *et al.* [1]. However, due to the difficulties in fabricating single crystals their intrinsic electronic properties are still under discussion [2–4]. Polycrystalline oxypnictides reveal very high upper critical fields and weak link behavior [5]. Multiband superconductivity is predicted from theoretical calculations [6] supported by experimental results on the upper critical field in polycrystalline La-1111 bulk samples [7] as well as on $SmFeAsO_{1-x}F_x$ and $NdFeAsO_{1-x}F_x$ single crystals [8] and, furthermore, nuclear magnetic resonance experiments [9]. As two distinct superconducting gaps were found in the oxypnictides [10] we simplify matters by considering only two major bands, created by electrons and holes, respectively. Regarding multiband superconductivity the anisotropy is of substantial interest. Calculations of average Fermi velocities in oxypnictides yield a high ratio $v_{xx}^2/v_{zz}^2 = 15$ [11] resulting in a large anisotropy of the effective electron mass γ_m. This large anisotropy value still has not been confirmed for $LaFeAsO_{1-x}F_x$ by experiments. Jia *et al.* [12] reported an anisotropy of the upper critical field, $\gamma_{H_{c2}}$, in $NdFeAsO_{1-x}F_x$ single crystals of around 5 near T_c. However, γ_m and $\gamma_{H_{c2}}$ in multiband superconductors cannot be considered equal as in the anisotropic Ginzburg-Landau theory for single band superconductors [13]. There, the relationship between anisotropies of electron masses, penetration depth, coherence length, and upper critical field can be expressed as $\gamma = \sqrt{\frac{m_c}{m_{ab}}} = \frac{\lambda_c}{\lambda_{ab}} = \frac{\xi_{ab}}{\xi_c} = \frac{H_{c2}^{\parallel ab}}{H_{c2}^{\parallel c}}$. Instead of this single anisotropy, it is necessary to distinguish between two anisotropies, $\gamma_\lambda = \lambda_c/\lambda_{ab}$ and $\gamma_{H_{c2}} = H_{c2}^{\parallel ab}/H_{c2}^{\parallel c}$ in order to understand the multiband character of pnictide superconductors [14].

The very high upper critical fields of pnictide superconductors rapidly exceed the capability of common high field measurement systems. Therefore, reliable information about the temperature dependence of H_{c2} and multiband calculations concerning the magnetic phase diagram are difficult to obtain [8]. The rather low superconducting transition temperature of the La-1111 system and, accordingly, the low upper critical fields compared to other oxypnictides make La-1111 thin films good candidates for studying the magnetic phase diagram and theoretical aspects, especially the mass anisotropy. In this work we document the anisotropic behavior and its temperature dependence by electrical transport measurements.

Our recent success in fabricating superconducting epitaxially grown La-1111 thin films of high crystalline quality [15] opens the way to study their basic properties. The samples were prepared using a standard high vacuum pulsed laser deposition setup at room temperature. An annealing process at $\approx 1000\,^\circ$C in evacuated quartz tubes initiates the $LaFeAsO_{1-x}F_x$ phase formation and leads to an epitaxially grown thin film. For a detailed description of the sample preparation please refer to [16,17]. In the following, we focus on the analysis of the critical current density, $J_c(T, B, \theta)$, and especially its angular dependence. Furthermore, the irreversibility field H_{irr} and the prevalent pinning mechanism are discussed. A comprehensive assessment of the film quality confirms textured growth and an absence of phase impurities, ensuring that none of the measurements are affected by grain boundaries or precipitates. Results of standard x-ray diffraction methods are provided in the supplemental material [18].

A scanning electron microscopy image of a focused ion beam cross section shown in Fig. 1(a) indicates that the La-1111 phase has a thickness of about 150 nm and grows sandwiched between two secondary phase layers. These

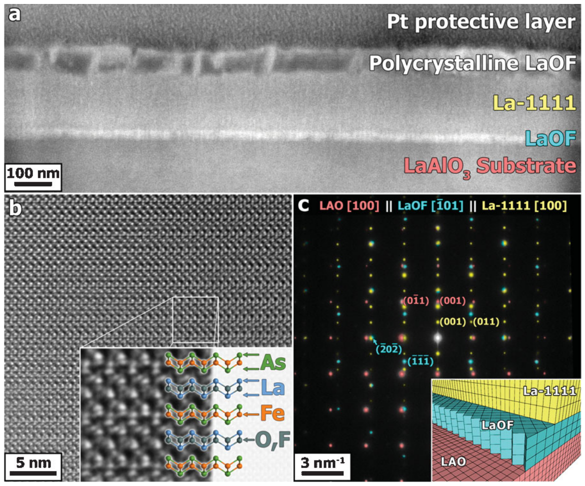

FIG. 1 (color). (a) $LaFeAsO_{1-x}F_x$ thin film cross section as prepared by focused ion beam. The approximately 150 nm thick epitaxial portion appears free of secondary phases and grows between two LaOF layers. (b) A representative high resolution TEM micrograph of the epitaxially grown La-1111 phase imaged along the [100] zone axis reveals highly crystalline growth without correlated defects. In the inset, the positions of the atomic columns are denoted. The image was Fourier filtered for noise reduction. (c) The artificially colored selected area diffraction pattern of the film cross section reveals the epitaxial relationship between $LaAlO_3$ substrate, the LaOF intermediate layer, and the La-1111 epitaxial phase.

can be identified as an epitaxially grown LaOF layer between the La-1111 film and the $LaAlO_3$ substrate as well as a polycrystalline surface layer (see Fig. 5 in the supplemental material [18]). The La-1111 layer itself is dense and appears to be free of secondary phases, which was subsequently confirmed by transmission electron microscopy (TEM). In Fig. 1(b), a representative yet very thin region of the La-1111 layer is shown indicating perfect single crystalline growth. The electron beam is parallel to the [100] zone axis revealing the La-1111 atomic structure. The positions of the atomic columns were determined by comparison of the raw data with contrast simulations. The epitaxial relationship between the various layers is documented by the selected area diffraction pattern in Fig. 1(c). The LaOF intermediate layer acts as a buffer for the La-1111 layer to relax its lattice misfit to the $LaAlO_3$ substrate.

Characteristic superconducting properties were investigated by means of electrical transport measurements, which is best accomplished using thin films since transport measurements of the critical current densities on single crystals is very challenging [19]. Critical current densities, $J_c(T, B, \theta)$, have been measured in four point geometry in maximum Lorentz force configuration. A standard J_c criterion of 1 μV cm^{-1} was applied (see Figs. 9 and 10 in [18]). At all temperatures, the critical current has a minimum at $B \parallel c$ (180°) and a maximum at $B \parallel ab$ (90° and 270°) as exemplarily shown in Fig. 2(a). The maxima at $B \parallel ab$ can be explained by intrinsic pinning because the coherence length ($\xi_{ab} \approx 3$ nm) is on the order of the spacing between the superconducting interlayer ($c \approx 0.8$ nm) [20,21]. Thin films of high-T_c cuprates grown by pulsed laser deposition often show a second local maximum at $B \parallel c$ due to correlated defects which arise from the columnar growth in physical vapor deposition methods. The absence of such a peak in our measurement as well as the absolute maximum values of J_c in the region of 10^5 A/cm^2 are in agreement with the microstructure observed by TEM. At this point it should be emphasized that the phase formation during the *ex situ* annealing process leads to a film growth with a high crystalline quality because the film growth during the annealing process is more similar to single crystal growth than to typical physical vapor deposition methods.

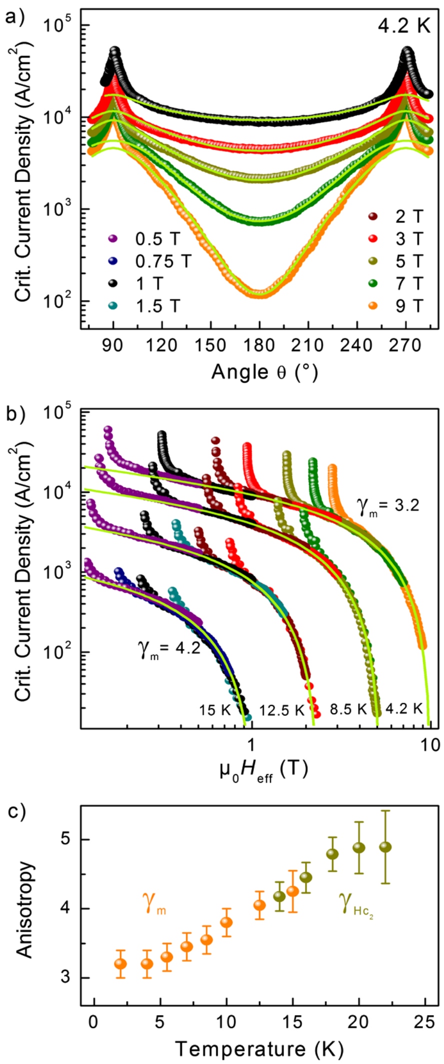

FIG. 2 (color online). (a) Angular dependence of the critical current density for several magnetic fields at 4 K. (b) Blatter scaling can be adopted for all temperatures with a temperature dependent effective-mass anisotropy γ_m. (c) Temperature dependence of the anisotropy determined from Blatter scaling of J_c data at low temperatures and from pulsed field H_{c2} anisotropy data at high temperatures.

It was shown for single band superconductors such as $YBa_2Cu_3O_{7-\delta}$ that the angular dependence of J_c can be scaled using an effective field $H_{\mathrm{eff}} = H\epsilon(\gamma_m, \Theta)$, where $\epsilon(\gamma_m, \Theta) = \sqrt{\sin^2\Theta + \gamma_m^{-2}\cos^2\Theta}$, and $\gamma_m^2 = m_c/m_{ab}$ is the anisotropy of the effective electron masses. This scaling behavior was theoretically predicted by Blatter, Geshkenbein, and Larkin [22], and experimentally verified on clean $YBa_2Cu_3O_{7-\delta}$ thin films [23] and on melt textured $YBa_2Cu_3O_{7-\delta}$ samples [24]. Since La-1111 is a multiband superconductor, different effective-mass anisotropies can be expected for the different charge carriers, holes, and electrons, in the individual bands, similar to MgB_2 [25–27].

As shown in Fig. 2(b) for four representative temperatures, J_c of La-1111 can be scaled by H_{eff} in a wide angular range around $B \parallel c$. From pinning force scaling, $F_p = J_c B$, $J_c(H_{\mathrm{eff}})$ can be recalculated and is plotted in Fig. 2(b) (solid green lines). With these fit functions, which also resemble J_c for $B \parallel c$, the anisotropy curves due to random defects can be recalculated as shown in Fig. 2(a) (solid green lines). Apart from intrinsic pinning due to the layered structure, the pinning centers—typically point defects—act isotropically and are randomly distributed. Since J_c scales in a large magnetic field range, the J_c anisotropy essentially reflects the mass anisotropy of the effective charge carriers.

Evaluating the effective-mass anisotropy from Blatter scaling shows a significant temperature dependence [Fig. 2(c)]. It ranges from 3.2 at 2 K to 4.2 at 15 K, the highest temperature at which we could reliably access J_c. At higher temperatures we were able to access $\gamma_{H_{c2}} = H_{c2}^{\parallel ab}/H_{c2}^{\parallel c}$, which was calculated from measurements in pulsed (up to 42 T, see Fig. 12 in [18]) as well as static (up to 9 T. see Fig. 13 in [18]) magnetic fields. The data at low temperatures, where H_{c2} is not accessible, and at high temperatures, where J_c is not accessible, join and overlap between 14 and 16 K indicating that the method of J_c scaling probes the anisotropy of H_{c2}. As a result, we can describe the J_c anisotropy within the theory of single band superconductors but with a temperature dependent effective-mass anisotropy. This assumption is valid if the two bands are weakly coupled as discussed below. We can distinguish between an electronic band dominating the properties at low temperatures, which has an effective-mass anisotropy of around 3, and another band dominating at higher temperatures with an anisotropy of around 5. It remains an open question which of the values of $\gamma_m \approx 3$ and $\gamma_m \approx 5$ can be related to electrons or holes.

Without line defects and anisotropic precipitates, as confirmed by TEM and supported by the J_c analysis, intrinsic and random pinning in oxypnictide superconductors can be studied. Moreover, iron pnictides are typical type-II superconductors similar to the high-T_c cuprates with a short coherence length ξ and a large penetration depth λ resulting in a large $\kappa = \lambda/\xi$. The flux lines show plastic behavior, especially in high magnetic fields, where the shear modulus, C_{66}, vanishes. Accordingly, the large trapping angle observed in the angular dependence of J_c can be explained by considering the plastic behavior of the flux lines. For high-κ superconductors the field dependence of C_{66} can be approximated by $C_{66} \propto (\frac{H}{H_{\mathrm{irr}}}) \times (1 - \frac{H}{H_{\mathrm{irr}}})^2$ [28].

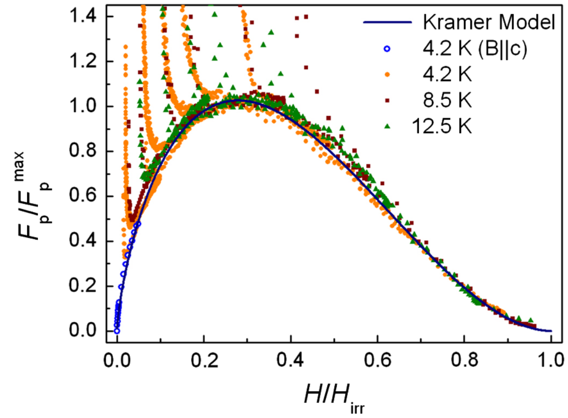

FIG. 3 (color online). The normalized pinning force, $F_p/F_{p\,\max}$, over normalized effective magnetic field, H/H_{irr}, scales in the entire temperature range. Hence, the pinning mechanism is temperature independent. Experimental data fit very well with the Kramer model ($p = 0.7$ and $q = 1.9$). Accordingly, J_c is limited due to the shear breaking of the flux lines.

In Fig. 3 the normalized pinning force, $F_p/F_{p\,\max}$, at various temperatures is plotted over the normalized effective field H/H_{irr}. For all temperatures, pinning forces scale for the region of random pinning; i.e., the pinning centers are randomly distributed and act isotropically. A functional relation is given by $F_p/F_{p\,\max} = K(\frac{H}{H_{\mathrm{irr}}})^p(1 - \frac{H}{H_{\mathrm{irr}}})^q$, where K is a proportionality constant and p and q are fitting parameters. Best fits were obtained with $p = 0.7$ and $q = 1.9$ (solid blue line). This fits very well the model proposed by Kramer for shear breaking of the flux line lattice $F_p/F_{p\,\max} \propto (\frac{H}{H_{\mathrm{irr}}})^{1/2}(1 - \frac{H}{H_{\mathrm{irr}}})^2$ [29]. As a result, the shear modulus C_{66} dominates the pinning force in the entire range of the applied magnetic field [30]. In spite of multiband superconductivity the pinning force density can be scaled at all temperatures with the same fitting parameters. Hence, the pinning mechanism is temperature independent.

Certainly, multiband superconductivity is manifested in the temperature dependent effective-mass anisotropy [Fig. 2(c)] as well as in the temperature dependence of the upper critical field. For the upper critical field parallel to the c axis, $H_{c2}^{\parallel c}$, we measured a steep upward curvature at low temperatures (Fig. 4). The applied magnetic fields were not high enough to completely study the upper critical field perpendicular to the c axis, $H_{c2}^{\parallel ab}$, in the low temperature region since $\mu_0 H_{c2}^{\parallel ab}$ exceeds 42 T at 14 K with a slope of $\frac{d\mu_0 H_{c2}^{\parallel ab}}{dT}|_{T_c} \approx -5$ T/K near T_c (see Figs. 11 and 12 in [18]).

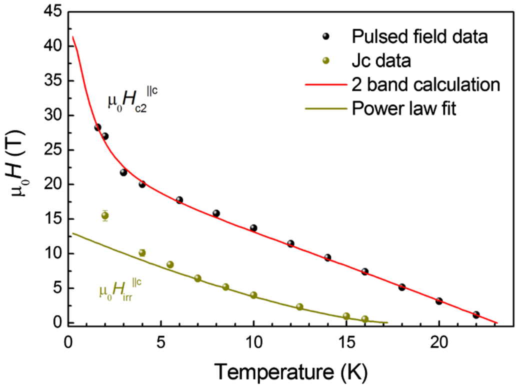

FIG. 4 (color online). The part of the magnetic phase diagram for $B \parallel c$ illustrates the steep increase of H_{c2} as well as H_{irr} at low temperatures. The experimental data can be described assuming a two band superconductor.

To describe the temperature dependence of H_{c2} we assume as the simplest case two bands, holes, and electrons, using a model calculation originally developed by Gurevich [27,31] for MgB_2. The transition temperature of the weaker band is near 6 K, where a large increase of $H_{c2}^{\|c}$ is observed. Similar to MgB_2, the steep increase in H_{c2} at low temperatures may be explained by two weakly coupled bands, one of them in the dirty limit. In the case of two weakly coupled bands the physics can be described as two shunted single band superconductors.

The temperature dependence of the irreversibility field is included in the magnetic phase diagram in Fig. 4. The data at very low temperatures were extrapolated from the pinning force scaling (Fig. 3) where H_{irr} is determined by the criterion of a vanishing pinning force. Additionally, we used Kramer plots ($J_c^{1/2}B^{1/4}$ vs B) to extrapolate the irreversibility fields. A steep increase of $H_{irr}^{\|c}$ can be seen at low temperatures in agreement with the steep increase of the upper critical field.

In summary, we have presented detailed electrical transport measurements on an epitaxially grown superconducting $LaFeAsO_{1-x}F_x$ thin film. The investigated sample reveals a clean $LaFeAsO_{1-x}F_x$ layer which is free of correlated defects. We have demonstrated that the critical current densities of oxypnictides can be scaled using the Blatter approach with a temperature dependent anisotropy. Because of the general evidence of multiband superconductivity in the oxypnictides, the mass anisotropy of a distinct band is experimentally difficult to access. Nevertheless, since the J_c anisotropy is scalable because of the temperature dependence of the upper critical field, we conclude that $LaFeAsO_{1-x}F_x$ has two major weakly coupled bands. This enables the evaluation of the mass anisotropies in the limits of low and high temperatures, respectively. We were able to explore the upper critical field parallel to the c axis in a large temperature range. The steep increase of the upper critical field as well as of the irreversibility field at low temperatures suggests the responsible band is in the dirty limit due to point defects. Accordingly, $LaFeAsO_{1-x}F_x$ shows a strong analogy to MgB_2. Combining H_{c2} data and the scaling of J_c we were able to deduce the temperature dependence of the effective-mass anisotropy, which cannot be measured directly due to the high upper critical fields of the oxypnictides.

This work was partially funded by the EU-FP6 Research Project NanoEngineered Superconductors for Power Applications (NESPA) No. MRTN-CT-2006-035619 and by the German Research Foundation (DFG) under Project No. HA 5934/1-1.

*Corresponding author.
M. Kidszun@ifw-dresden.de

[1] Y. Kamihara, T. Watanabe, M. Hirano, and H. Hosono, J. Am. Chem. Soc. **130**, 3296 (2008).
[2] J. Karpinski *et al.*, Physica (Amsterdam) **469C**, 370 (2009).
[3] J. Q. Yan *et al.*, Appl. Phys. Lett. **95**, 222504 (2009).
[4] C. de la Cruz *et al.*, Nature (London) **453**, 899 (2008).
[5] S. Haindl *et al.*, Phys. Rev. Lett. **104**, 077001 (2010).
[6] H. Eschrig and K. Koepernik, Phys. Rev. B **80**, 104503 (2009).
[7] F. Hunte *et al.*, Nature (London) **453**, 903 (2008).
[8] J. Jaroszynski *et al.*, Phys. Rev. B **78**, 174523 (2008).
[9] S. Kawasaki *et al.*, Phys. Rev. B **78**, 220506(R) (2008).
[10] R. S. Gonnelli *et al.*, Phys. Rev. B **79**, 184526 (2009).
[11] D. J. Singh and M. H. Du, Phys. Rev. Lett. **100**, 237003 (2008).
[12] Y. Jia *et al.*, Appl. Phys. Lett. **93**, 032503 (2008).
[13] V. G. Kogan, Phys. Rev. Lett. **89**, 237005 (2002).
[14] S. Weyeneth *et al.*, J. Supercond. Novel Magnetism **22**, 347 (2009).
[15] M. Kidszun *et al.*, Supercond. Sci. Technol. **23**, 022002 (2010).
[16] E. Backen *et al.*, Supercond. Sci. Technol. **21**, 122001 (2008).
[17] M. Kidszun *et al.*, Europhys. Lett. **90**, 57 005 (2010).
[18] See supplemental material at http://link.aps.org/supplemental/10.1103/PhysRevLett.106.137001 for experimental details and additional information.
[19] P. Moll *et al.*, Nature Mater. **9**, 628 (2010).
[20] J. Jaroszynski *et al.*, Phys. Rev. B **78**, 064511 (2008).
[21] M. Tachiki and S. Takahashi, Solid State Commun. **72**, 1083 (1989).
[22] G. Blatter, V. B. Geshkenbein, and A. I. Larkin, Phys. Rev. Lett. **68**, 875 (1992).
[23] L. Civale *et al.*, J. Low Temp. Phys. **135**, 87 (2004).
[24] D. Braithwaite *et al.*, J. Low Temp. Phys. **92**, 295 (1993).
[25] H. J. Choi *et al.*, Nature (London) **418**, 758 (2002).
[26] M. Angst *et al.*, Phys. Rev. Lett. **88**, 167004 (2002).
[27] A. Gurevich, Physica (Amsterdam) **456C**, 160 (2007).
[28] E. H. Brandt, Phys. Rev. B **34**, 6514 (1986).
[29] E. J. Kramer, J. Appl. Phys. **44**, 1360 (1973).
[30] E. H. Brandt, Phys. Rev. B **71**, 014521 (2005).
[31] A. Gurevich, Phys. Rev. B **67**, 184515 (2003).